Annu. Rev. Phys. Chem. 2006. 57:527–54
doi: 10.1146/annurev.physchem.57.032905.104521

First published online as a Review in Advance on January 16, 2006

RAMAN CRYSTALLOGRAPHY AND OTHER BIOCHEMICAL APPLICATIONS OF RAMAN MICROSCOPY

Paul R. Carey
Department of Biochemistry, Case Western Reserve University, Cleveland, Ohio 44106; email: paul.carey@case.edu

Key Words transcarboxylase, drug screening, β-lactamase, amyloid Aβ, α-synuclein

■ **Abstract** Recent studies using a Raman microscope have shown that single protein crystals provide an ideal platform to undertake Raman difference spectroscopic analyses under nonresonance conditions. This approach, termed Raman crystallography, provides a means of characterizing chemical events within the crystal such as ligand binding and enzyme reactions. In many cases Raman crystallography goes hand in hand with X-ray crystallographic studies because the Raman results can inform the X-ray crystallographer about the status of chemical events in the crystal prior to flash freezing and X-ray analysis. In turn, the combined data from the Raman and X-ray analyses are highly synergistic and offer novel perspectives on structure and dynamics in enzyme active sites. In a related area, protein misfolding, Raman microscopy can provide detailed insights into the chemistry of the amyloid plaques associated with Alzheimer's disease and into the intermediates on the α-synuclein protein misfolding pathway implicated in Parkinson's disease.

INTRODUCTION

Raman microscopy can provide exquisite molecular detail on the events occurring in protein crystals and other protein-based bodies. Although Raman microscopy can be used for vibrational imaging (1, 2), this review deals specifically with systems where Raman spectroscopic data are collected from a single micron-sized focal volume. For single crystals the focal volume is within the crystal, and the resultant Raman scattering reports on events occurring within that volume. The experiments usually involve soaking in a ligand and recording the Raman difference spectrum of the crystal [(Raman spectrum of the protein-ligand complex) minus the (Raman spectrum of the protein)] as a function of time. Typically, under "normal" (nonresonance) Raman conditions, a data set is collected every minute. The difference data allow the experimentalist to do the following:

- Monitor the ligand soaking into (or out of) the crystal and measure the concentration inside the crystal.
- For ligands that form noncovalent complexes, reach conclusions on ligand-active site interactions.
- For ligands that are substrates, follow the course of the chemical reaction occurring inside the crystal, such as the rise and fall of enzyme-substrate intermediates.

These studies interface synergistically with X-ray crystallography, and the combined spectroscopic/crystallographic approach is a powerful new weapon in the structural biologist's armamentarium. The Raman data inform the X-ray crystallographer on the status of the crystal during ligand soak-in or soak-out experiments or, for example, the population of unstable complexes within the crystal, thus providing the conditions for optimal flash freezing prior to X-ray data collection. At the same time the combined Raman and X-ray data offer unique insights into the static and dynamic aspects of events involving the ligand and the protein.

Single protein crystals provide an impressive example of correct protein folding and three-dimensional array formation. However, Raman microscopy is used to show that during some ligand soaking-in experiments, proteins within crystals can undergo massive, and unexpected, conformational changes and assume largely β-sheet secondary structure, mimicking the end point of protein misfolded entities found in disease states. This provides a link to the second major topic in this review: use of Raman microscopy to elicit chemical insights into β-sheet structures found in the amyloid plaques isolated from the brains of deceased Alzheimer's patients. Raman microscopy is also used to provide novel information on intermediates formed on the misfolding pathway of the protein α-synuclein that lead to aggregates that play a major role in the progression of Parkinson's disease. A key aspect of the latter studies involves synergy between two techniques. Atomic force microscopy is used to define the shape and size of α-synuclein aggregates in vitro, whereas Raman microscopy on the same samples probes protein secondary structure.

RAMAN CRYSTALLOGRAPHY

Apart from its intrinsic intellectual interest, the need to follow ligand binding and chemical reactions in single protein crystals by a simple method has been driven by the great upsurge in protein crystallography. Basically, it would be of high value to crystallographers if processes occurring within crystals could be defined before the crystal structure is solved. Over the past few decades, most classical optical techniques, such as absorption and fluorescence spectroscopies, have been utilized to this end (3), although these techniques necessarily have been restricted to systems that involve a chromophore or a chromophoric label. Similarly, infrared spectroscopy has been used to follow events in protein crystals (4), although, again, general applicability is limited because many regions in the infrared

fingerprint range are essentially inaccessible as a result of the high optical density of the protein in those regions. In contrast, Raman microscopic studies on single crystals, usually involving ligand-soaking experiments and the Raman difference spectroscopic approach under nonresonance Raman conditions, overcome many of these restrictions and provide a general, widely applicable means of following chemistry within crystals (5). Indeed, the crystal becomes akin to a well-defined, miniature laboratory in which experiments in protein chemistry and enzymology can be undertaken. Of course, there may be limitations: Active sites may be blocked by protein-protein contacts in the crystal precluding binding studies, and protein dynamical motions, necessary for protein function, may be damped within the protein array. However, these problems have been encountered infrequently in our early studies and are usually outweighed by the synergy resulting from combined spectroscopic and crystallographic studies on the same crystals. At present it normally requires 1 min or more to acquire a Raman spectrum with an acceptable signal-to-noise ratio, so only slow enzyme substrate reactions can be studied in crystals.

Although future work will undoubtedly involve nucleic acid and receptor arrays, most of the recent studies in Raman crystallography involved protein-based enzymes. In enzymology, the Raman, or resonance Raman, spectrum of a substrate bound to an enzyme's active site can be the source of unique mechanistic insights (6–8). However, in the absence of a chromophoric substrate to provide an intensity-enhanced spectrum, the Raman spectrum of the substrate is often obscured by the thousands of vibrational modes from the protein. In their pioneering work, Deng & Callender (8 and references therein) showed that this restriction can be overcome in part by using a difference spectroscopic approach. By subtracting the Raman spectrum of the enzyme from that of the enzyme-substrate complex, the Raman spectrum of the bound substrate is revealed—along with some contributions from protein modes if substrate binding brings about protein conformational change. Because the difference approach involves detecting the minute contribution of the substrate to the composite enzyme-substrate spectrum, the parent spectra have to have a high signal-to-noise ratio and be stable. In practice, these requirements become a severe limitation to general applicability for proteins in solution. However, we have shown recently that use of single crystals provides an ideal platform for the Raman difference approach. With the use of a Raman microscope, very high signal-to-noise ratio data sets that have low and stable underlying spectral backgrounds are obtained. Thus, it has become almost routine in our laboratory to "follow" ligands soaking into crystals, via the Raman difference spectrum, occurring at room temperature on the timescale of tens of seconds.

Early Studies on Protein Crystals

Although the use of a Raman microscope to obtain nonresonance Raman difference data from crystals is a recent innovation, spectroscopists realized soon after the introduction of the laser that single-crystal Raman spectroscopy was feasible. In the early 1970s, Yu and coworkers (9) compared the crystal and solution

Raman spectra for proteins such as α-lactalbumin, insulin, and glucagon. In these studies, single protein crystals were mounted in a cuvette or glass vial and positioned by eye at the focal point of the fore-optics, that is, directly at the front of a standard Raman instrument, which was a double monochrometer with a single photomultiplier detector. The work provided some of the earliest evidence that the main-chain structures of proteins in crystals are similar to those in solution and that crystallization has no detectable effect on the backbone conformation. Small differences observed between crystal and solution Raman data were interpreted in terms of changes in amino-acid side-chain conformations. In a similar way, resonance Raman spectroscopy was used to study the heme moieties in cytochrome P450 and myoglobin protein crystals (10, 11). The active site heme structures are identical for the crystal and solution phases. In the 1980s and 1990s, new technologies permitted the development of Raman microscopy, where an optical microscope is coupled to a Raman spectrometer to collect Raman signals from sample regions as small as a few micrometers. Researchers found applications for Raman microscopy in cell biology (12, 13) as well as in heme-protein crystal studies. Most of the latter involved the peroxidase family (14), and because these studies were carried out under resonance Raman conditions, very low laser power had to be used to minimize photodegradation induced by the laser beam. A handful of nonresonance Raman microscopic studies of protein crystals were reported in the 1980s and 1990s. For example, G.J. Thomas's group found small differences in the Raman intensities of side chains of subunits in the empty capsid of bean pod mottle virus (15) and in the *Ff* gene V protein (16) in crystalline and solution states. These differences were interpreted as the result of changes in a small number of side-chain environments between crystal and solution, creating a parallel to Yu's early work. In a study of crystalline DNA-protein complexes, Peticolas and coworkers (17) detected major changes in the conformation of an oligonucleotide d(TCGCGAATTCGCG) binding to the restriction endonuclease *Eco*RI. Following these studies, two important technical advances were introduced in the 1990s: (*a*) red-light sensitive charge-coupled photon detectors and (*b*) holography-based notch filters that block unwanted elastically scattered photons. Together, these innovations greatly increased the sensitivity of Raman microscopes in the red (600- to 800-nm) region of the spectrum. This was a critical breakthrough because the Raman microscope could now be operated using laser excitation in the red part of the spectrum, thereby providing protein spectra free from the weak luminescence background that often accompanies excitation in the blue/green (near 500 nm). Thus, it became feasible to carry out "chemistry in crystals," to follow the consequences of inhibitors soaking into crystals and binding in enzyme active sites, and to monitor enzyme-substrate reactions occurring on a slow timescale (tens of seconds). The improvements in spectral sensitivity meant that these studies could be undertaken under nonresonance Raman conditions, eliminating the possibility of the laser beam driving unwanted and uncontrolled photochemistry, as often occurred during resonance Raman experiments (18).

Raman Data from Crystals In Situ

An important advantage of a Raman microscope is that data can be obtained in situ under the conditions used to grow the crystals in microliter-sized drops. Subsequently, the concentrations of species inside the drops can be varied to soak-in or soak-out ligands. A schematic of a Raman microscope is shown in Figure 1. Crystals are usually grown in, or transferred to, hanging drops in a 24-well plastic tray of the kind used by X-ray crystallographers. The tray is placed on the microscope stage, and the crystal in each drop can be viewed via a long focal length objective and a video charge-coupled device (CCD) camera for optical imaging. A laser beam is introduced on the microscope's optical axis using a fiber optic, and the beam focused on the crystal can be viewed on the computer monitor. This configuration provides the degree of experimental control needed because

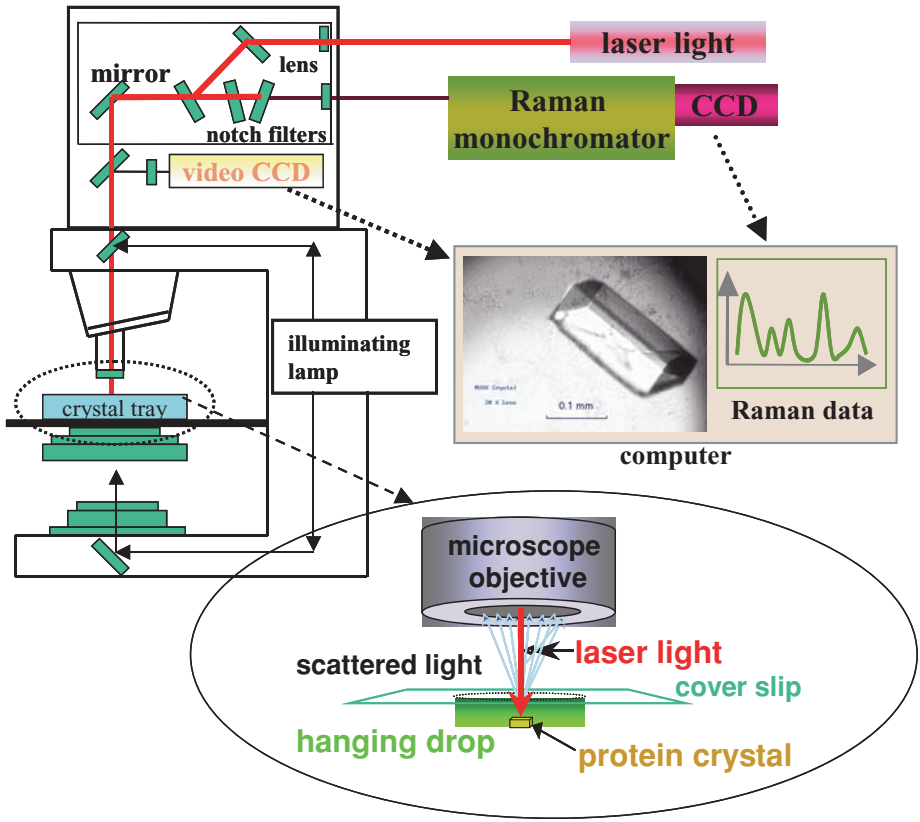

Figure 1 Raman microscope coupled to a krypton laser and a spectrometer. Both video images and spectral data can be displayed in real time on the computer screen. Also shown is a magnified view of a protein crystal in a hanging drop under the microscope objective.

the crystals and focal spot are usually too small (on the tens of micrometers scale) to be viewed by the naked eye. In the next step the standard illuminating source is blocked and the back-scattered light from the focal spot goes back through the microscope and, via optical filters and a second fiber optic, is fed into a Raman spectrograph. The Raman spectral image at the CCD photon detector then appears on the computer monitor providing the Raman spectrum associated with the focal spot on the crystal. At present, the microscope is operated in the nonconfocal mode to maximize light throughput, and the focal volume is typically 20 μm in diameter and 30 μm in depth; these conditions determine a minimal crystal dimension of 30 μm for optimal spectral quality. For most systems, approximately100 seconds are required to collect a complete data set, using 100 mW of 647.1 nm Kr^+ laser excitation at the sample. At these power levels, the temperature of the crystal increases by approximately 15°C when it sits in a 5-microliter bath. The crystal appears to be stable, and burning or other damage has not been observed. While undertaking Raman difference spectroscopy, researchers must exercise care to avoid perturbing the crystal when introducing the ligand into the liquid surrounding the crystal. The ideal situation is one in which the Raman spectra before and after the soaking are essentially superimposable, giving rise to the highest quality Raman difference data. It is important to bear in mind that the intensity of Raman scattering may be dependent on the relative orientations of the crystal axes and the laser beam, a factor that can be used to facilitate the Raman difference method (19), but which can also lead to uncontrolled changes in Raman intensity, if not taken into account (20).

During the past few years, we instigated several projects with the goal of characterizing enzyme-ligand complexes via Raman difference spectroscopy. We examined substrates binding to the subunits of the enzyme transcarboxylase and, separately, the reaction between β-lactamase and various suicide substrates that are important pharmaceuticals for treating bacterial infections. The initial studies for these systems were undertaken in solution, but we were unable to generate high-quality difference spectra. However, upon repeating these trials in single crystals of the target enzyme, we obtained excellent reproducible data and the projects became feasible. A comparison between the conditions found in solution and those in single crystals demonstrates why superior results are obtained from crystals:

- **Concentration**. Depending on their molecular weight, proteins are usually in the 15- to 55-mM concentration range in crystals. In solution, it is often difficult to achieve concentrations in the 0.5- to 1-mM range. Thus crystals have an immediate concentration advantage of a factor of 10 to 100.
- **Spectral background**. In aqueous solution, water contributes a Raman spectrum that essentially forms a continuum in the fingerprint region. This is of weak intensity but becomes an issue at low solute concentrations. In crystals, this background decreases by an order of magnitude relative to the protein spectrum. In addition, aggregated protein in solution leads to strong Rayleigh scattering that "bleeds over" into the Raman regime. Transparent

crystals show less Rayleigh scattering. Finally, most proteins have a weak luminescent spectrum that helps obscure the Raman scattering. This may be due to a minute fraction of proteins whose amino-acid side chains have undergone a chemical reaction to produce a fluorophore (akin to the green fluorescent protein). These spontaneously modified protein molecules are difficult to separate from pure protein and are undetectable by most analytical techniques. On the other hand, the luminescence is minimal when red excitation is used for the Raman spectrum and appears to be partially quenched in crystals compared with solution.

- **Resolution**. In crystals, protein (and ligand) vibrational band shapes narrow, and a better baseline resolution is achieved compared with solution. This we ascribe to the damping of large-scale protein vibrational motions in the crystal as a result of protein-protein contacts.
- **Ligand concentration**. In solution, for Raman difference studies, protein must be greater than or equal to ligand concentration to avoid spectral interference from unbound ligands. A crystal may be soaked with a ligand that is 5 mM or more in the surrounding drop, which reaches 30 mM for the bound ligand in the crystal (if this is the concentration of active sites). Unbound ligand concentration in the crystal is typically 2 mM and gives weak, if any, features. Thus, interference from unbound ligands is less of a problem in the crystal compared with solution studies.

Compared with solution studies, Raman crystallography has other advantages that are not related to data quality. These include the ability to undertake competitive inhibition experiments in the crystal and the ability to quantitate the amount of ligands in the crystal and thus the number of ligands present per protein unit. Some examples are given below. Another potential advantage stems from the tensorial nature of Raman scattering. In some cases, where the active sites are in a uniform orientation, a study of polarized Raman scattering (20) from the crystal can provide information on the orientation, with respect to the crystal axes, of the ligand bound in the active site. This application has not been explored in detail.

Enzyme-Substrate and Enzyme-Inhibitor Reactions

This section deals with three enzyme systems, transcarboxylase, urokinase, and a β-lactamase, where each exemplifies different principles. However, at first we discuss the simple but important finding that Raman crystallography can monitor ligands soaking into crystals and usually quantitate the amount present.

OBSERVING AND QUANTITATING LIGANDS SOAKING INTO CRYSTALS Raman difference spectra can be used to follow the introduction of ligands into the crystals by soaking-in, or their removal by soaking-out. For the former, the ligand is added to the mother liquor surrounding an apo-crystal to give a final concentration in the 5–15 mM range. By recording sequential Raman difference spectra from the

crystal, features from the ligand are seen to increase in intensity with time until all the enzyme active sites are occupied. As an example consider the binding of substrate to the 12S subunit of the enzyme transcarboxylase (21). Transcarboxylase is a multisubunit enzyme that catalyzes the overall transfer of carboxylate from methylmalonyl-CoA (MM-CoA) to pyruvate to form oxaloacetate and propionyl-CoA. In the first half of the reaction the 12S subunit transfers a carboxylate group from MM-CoA to a biotin group on transcarboxylase's 1.3S subunit:

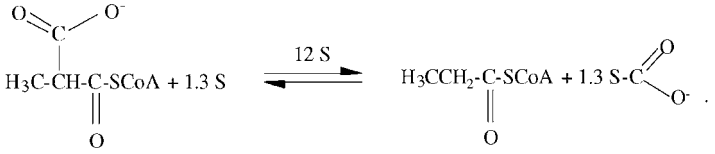

1.

12S functions as a hexamer in solution with a total molecular weight of 336,000 Da, and single crystals of the protein retain the hexameric motif (22). The MM-CoA substrate can be soaked into the crystal, and in the absence of 1.3S-biotin, no reaction occurs. The most intense modes in the Raman spectrum of MM-CoA in Figure 2*A* are due to the adenine moiety on CoA because adenine is a strong Raman scatterer. The adenine feature at 724 cm^{-1} can be used to follow the time course of soaking-in (23). In a 5-mM bath of ligands, the 724 cm^{-1} band increases in intensity as MM-CoA penetrates the 12S crystal and reaches a saturation level in approximately 1 h. Unbound ligand concentration within the crystal is essentially undetected because it is present at less than 2 mM—a concentration that gives very weak signals under the Raman microscope. Thus, the intensity of the 724 cm^{-1} peak is directly proportional to the concentration of MM-CoA bound to active sites in the enzyme crystal. Using a standard plot of intensity versus concentration for free MM-CoA in solution, the intensity of the 724 cm^{-1} crystal feature yields 11.5 mM MM-CoA in the crystal. [This approach is valid only for crystal complexes that do not show a strong dependence of Raman intensity on crystal orientation, which is the case here owing to at least six separate orientations of the MM-CoA molecules in the crystal (22)]. The X-ray crystallographic data show that the concentration of the 12S hexamer in the crystal is 2 mM, i.e., 12 mM in monomer. Thus, a stoichiometric 1:1 complex has formed between MM-CoA and each monomer.

By replacing MM-CoA–containing mother liquor with substrate-free mother liquor or 60% ammonium sulfate solution, soaking-out, i.e., gradual removal of the MM-CoA, occurs, and the 724 cm^{-1} band becomes undetectable after 30 to 60 min. These findings were quite useful in efforts to solve the three-dimensional structure of 12S complexes. Initially, 12S was cocrystallized with MM-CoA, but in the resultant structure, although the CoA could be seen, electron density from the MM group was absent. As it turned out, in the several weeks taken for the crystallization process, the MM group was removed from the CoA by slow hydrolysis. However, guided by the Raman results, CoA was soaked-out, and fresh MM-CoA soaked-in for only 1 h. The crystals were flash frozen, and now electron density could be observed clearly for the MM moiety in the active site. Consonant with the Raman difference data, there are 6 MM-CoAs bound per 12S hexamer (22).

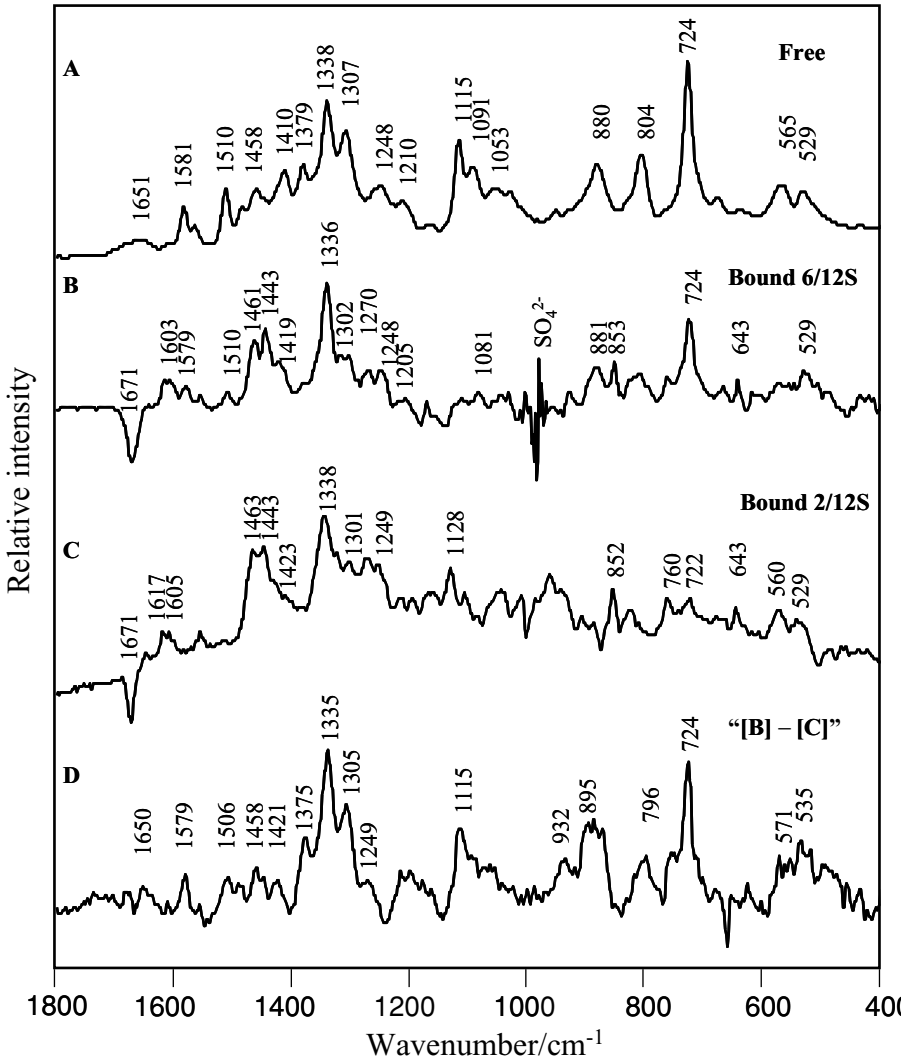

Figure 2 Raman difference spectra of methylmalonyl-CoA. (*A*) [3.5 mM MM-CoA in water] minus [water]. (*B*) [MM-CoA bound to a single crystal of 12S, six molecules substrate per hexamer] minus [apo crystal]; the derivative feature near 980 cm^{-1} is due to the presence of sulfate anions. (*C*) [MM-CoA bound to a single crystal of 12S, two molecules substrate per hexamer] minus [apo crystal]. (*D*) MM-CoA bound to a single crystal of 12S, obtained by subtracting [2MM-CoA-12S] from [6MM-CoA-12S]. These spectra were generated from the same crystal by a soaking-out experiment.

MM-CoA is a fairly large molecule and takes up to 1 h to diffuse fully into a 12S crystal. In other systems smaller ligands can be introduced more rapidly. For example β-lactams diffuse fully into β-lactamase enzyme crystals in approximately 1 min (24). Of course, other factors such as solvent channel size and active site accessibility affect soak-in times.

COOPERATIVE CONFORMATIONAL CHANGE INDUCED BY MM-COA BINDING TO 12S Binding of MM-CoA to the active sites within a 12S crystal leads to a modest conformational change in the protein (23). This conformational change results in a change in the protein's Raman spectrum, consequently in the Raman difference spectrum [(protein + ligand) minus (protein)], the protein modes do not subtract to zero. Although, in this kind of experiment, ligand modes always appear in the positive direction (above the baseline), protein features can appear in the positive and negative directions. This is seen clearly in the Raman difference spectrum in Figure 2*B*, where many protein features have been assigned to peptide group motions and to aromatic side chains (whose environments have been modified by MM-CoA binding) (23). Most band assignments are accurate as they are based on 30 years of knowledge available in the protein-Raman literature and extensive recent studies in Raman crystallography. One limitation of the data on conformational change is that unless site-directed isotope editing is used (25), it is not possible to pinpoint the region where the protein conformational change occurs. However, the intensity of the amide modes in the difference spectra allows us to estimate that the conformational change involves only a few percent of the total peptide linkages.

As discussed above, the adenine peak near 724 cm^{-1} can be used to quantitate the amount of bound MM-CoA, and accordingly the intensity of this feature in Figure 2*B* allows us to calculate that there are 6 MM-CoAs per hexamer, resulting from a prolonged soaking-in experiment. During a separate soak-out experiment Figure 2*C* shows that only two molecules of MM-CoA are left in each 12S hexamer. Although intensity of the ligand modes is greatly reduced, the protein bands in the difference spectrum are unchanged. This was an early indication that MM-CoA binding brings about a cooperative change in protein conformation. This has been confirmed by carefully titrating MM-CoA into crystals of 12S (X. Zheng & P. Carey, unpublished work). A complete conformational change occurs upon binding the first MM-CoA per hexamer, and no further change is observed upon binding the next five ligands in the hexamer. The cooperative conformational change is linked intimately with the labile $–COO^-$ group on the methylmalonyl group because binding of propionyl-CoA (the product; see Equation 1) does not bring about a conformational change. By subtracting the difference spectra (Figure 2*B*,*C*), we eliminate the protein modes and generate the spectrum of only bound MM-CoA without any contribution from the protein; this is seen in trace Figure 2*D*.

COMPETITIVE INHIBITION AND DRUG SCREENING If drug targets form crystals that are amenable to soak-in, soak-out experiments, Raman crystallography can

be used to facilitate the search for the most effective inhibitor. This was first demonstrated using urokinase, a trypsin-like human serine protease. Urokinase has been shown to be strongly associated with tumor cells and to play a role in basement membrane degradation. Furthermore, inhibitors of the enzyme have been reported to slow tumor metastasis as well as the growth of the primary tumor. Thus, urokinase has been a target for potent inhibitors that could be valuable in cancer therapy. One family of inhibitors developed at Abbott Laboratories is based on naphthamidine as the parent compound and five derivatives of the family are shown in Scheme 1.

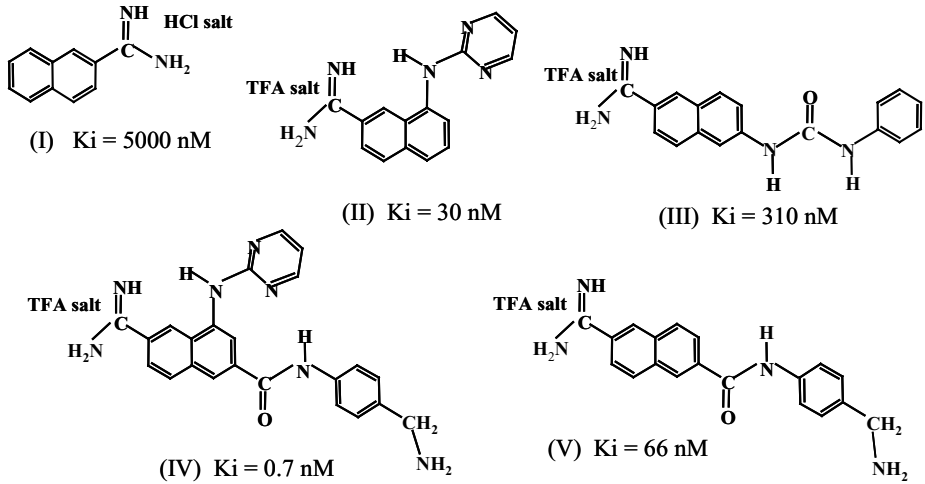

Scheme 1 Urokinase inhibitors: structures and inhibition constants.

Using crystals supplied by our collaborators at Abbott, we were able to obtain Raman spectra for all five inhibitors, bound individually to crystals of urokinase. The data generated for each complex are markedly superior to those obtained in solution (26). All difference spectra of the bound inhibitors contain bands from the naphthyl ring and amidine group, as well as other functional groups. The Raman modes could be reproduced by quantum-mechanical analysis, giving a firm interpretation or prediction of the experimentally observed bands. In particular, the calculations indicated that protonation of the amidine group gives rise to a marker band near 1525 cm^{-1}. All complexes show this marker band, demonstrating that the amidine is protonated (e.g., see Figure 3), information that could not be obtained directly from X-ray crystallographic analysis. In a screen-type experiment, a mixture containing equimolar amounts of each of the five inhibitors was added to the mother liquor containing a single urokinase crystal. The system was allowed to equilibrate fully before transferring the crystal with bound ligands to fresh mother liquor and obtaining the Raman spectrum. The difference spectrum in Figure 3 contains almost exclusively features of compound IV, indicating that this is the most potent inhibitor in the group studied. Marker bands from the other inhibitors, whose

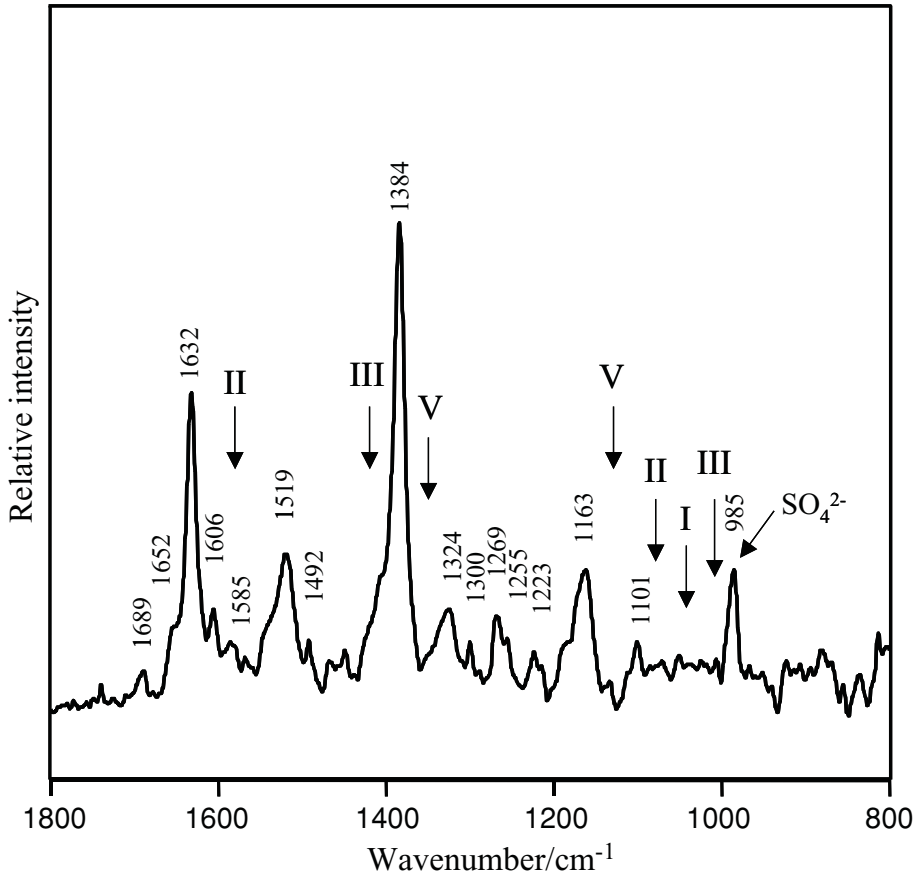

Figure 3 Results of a competitive inhibition experiment. Raman difference spectrum of inhibitor(s) bound to urokinase crystal, derived from soaking in a mixture of five inhibitors. The Raman spectra provide unique evidence for protonation of the amidine group.

peaks are expected at the arrow positions shown on Figure 3, are not detected. The finding that compound IV is the best inhibitor is consonant with the K_i values determined individually in solution. This result suggests that the active site in the crystal is readily accessible via solvent channels. Figure 3 demonstrates that Raman crystallography can be used to screen for the most effective inhibitor, at the same time the spectroscopic data provide some insight into the chemistry of binding.

ENZYME-SUBSTRATE REACTIONS WITHIN CRYSTALS: β-LACTAMASES AND DRUG RESISTANCE Raman crystallography can identify and follow the populations of reaction intermediates in single crystals. At the present stage of technology, for this approach to be effective, the reactions have to occur on timescales of longer than 1 min, which is set by the need to accumulate the Raman data for 1 min or more on

the CCD detector. The other complication arises from possible population heterogeneity in the crystal caused during substrate soak-ins by the reaction occurring near the surface of the crystal prior to substrate reaching the middle of the crystal. However, if these limitations do not apply, or can be overcome, the approach is powerful.

At this time, the best-developed example concerns β-lactamase enzymes reacting with three drugs that are used widely in medicine (27, 28). Penicillin and its analogs kill bacteria by interfering with cell-wall synthesis. However, bacteria produce enzymes, β-lactamases, that hydrolyze penicillin before it can attack the bacterium. Therefore, it is standard clinical practice to deliver a second drug with penicillin that will block the active site of the β-lactamase. However, as a response, bacteria produce mutated forms of β-lactamase that are not blocked by the inhibitor drug. This response is a major source of drug resistance. A main goal of the Raman crystallographic analysis of β-lactamase-drug reactions is to compare the reactions involving wild-type and mutant enzymes and thus elucidate the molecular determinants of drug resistance.

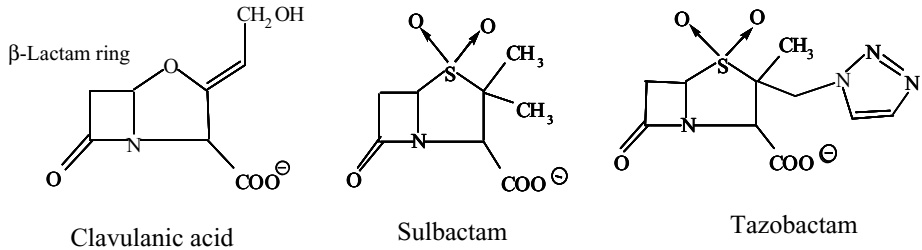

Scheme 2 Structure of β-lactamase inhibitors.

The three commonly used β-lactamase inhibitors are shown in Scheme 2. They are known as suicide, or mechanism-based, inhibitors because they react chemically with the enzyme via a complex-reaction pathway. Although this pathway has been mapped out in some detail over the past 30 years, key questions remain unresolved. In the context of drug resistance, which species on the reaction pathway are the most effective in inhibiting the enzyme, and do single-site mutations affect the structure or populations of intermediates, or both of these properties? These reactions can be studied by Raman crystallography because important intermediates are formed on the timescale of minutes to tens of minutes and because the substrates soak into the crystals in approximately 1 min, minimizing the effect of kinetic heterogeneity within the inner and outer layers of the crystal. Initial studies utilized a single mutated form of the enzyme E166A that has a deacylation step on the pathway blocked by replacing E166 by alanine. Thus, the intent was to focus initially on the acyl-enzyme species occurring in the reaction scheme (24).

In an individual experiment one of the compounds shown in Scheme 2 is infused into an E166A lactamase crystal. The corresponding Raman difference spectra contain features that can be assigned to a reaction intermediate involving the drug

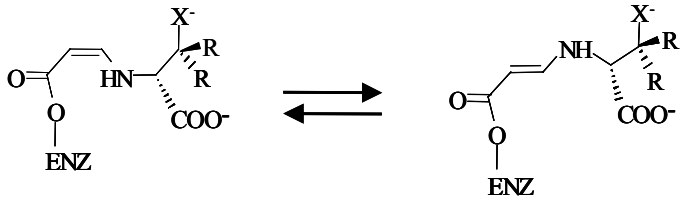

Scheme 3 Two possible acyl-enzyme enamine species in E166A lactamase crystal.

in the enzyme's active site. However, the spectra also show that the drug has undergone drastic chemical changes. A key observation is that there is no trace of the lactam C═O stretch near 1780 cm^{-1} seen in the parent compound showing that lactam ring opening has occurred within the dead time of our experiment—essentially 2 min. In the case of sulbactam or tazobactam, intense C-S stretching modes from the thiazolium ring are absent in the spectra of the reacting species. This shows that the five-membered thiazolium ring has opened, too. However, in each case a peak grows in with time near 1595 cm^{-1} (24); detailed analysis using NH to ND exchange and quantum-mechanical calculations assigned this feature to a stretching vibration from the *trans*-enamine species (see Scheme 3), and this intermediate is formed by a complex rearrangement of the drug in β-lactamase's active site. We found that all three inhibitors showed a peak in this region, and we

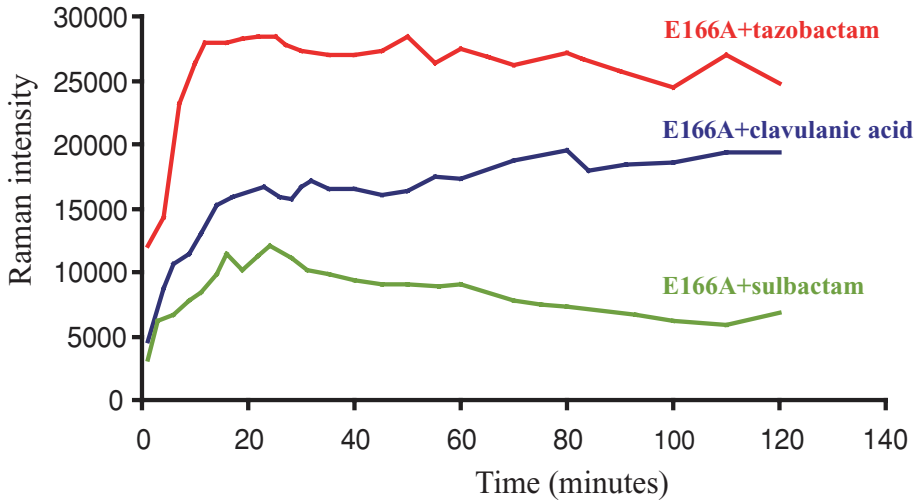

Figure 4 Time dependence of enamine peak height near 1593 cm^{-1} (normalized to the amide I band) for the E166A crystal and three inhibitors in H_2O. Red: tazobactam; green: sulbactam; blue: clavulanate.

were able to use the peak-intensity variation to follow population changes for the intermediates in the crystal. These changes are shown in Figure 4. Interestingly, tazobactam, the compound with the greatest clinical efficacy among the targeted inhibitors, has the highest buildup of the *trans*-enamine species.

It is of very great value for X-ray crystallographic studies to be able to follow population changes in crystals. Prior to the Raman crystallographic analysis, crystallographers frequently flash froze crystals to trap intermediates during soak-in experiments. However, this was necessarily much on a hit-or-miss basis. Now, however, Raman data can guide the conditions and time for flash freezing. Figure 4 shows that the putative enamine population for tazobactam reaches a maximum at approximately 28 min. Using the 28-min soaking time, our crystallographer colleagues were able to trap, for the first time, a stoichiometric [tazobactam–β-lactamase] complex with one *trans*-enamine per active site (29). A diagram of the active site derived from this structure is shown in Scheme 4. The structure reveals favorable interactions involving tazobactam's SO_2 group and triazolyl ring. However, sulbactam lacks a triazolyl ring, and clavulanic acid lacks both the ring and an SO_2 group.

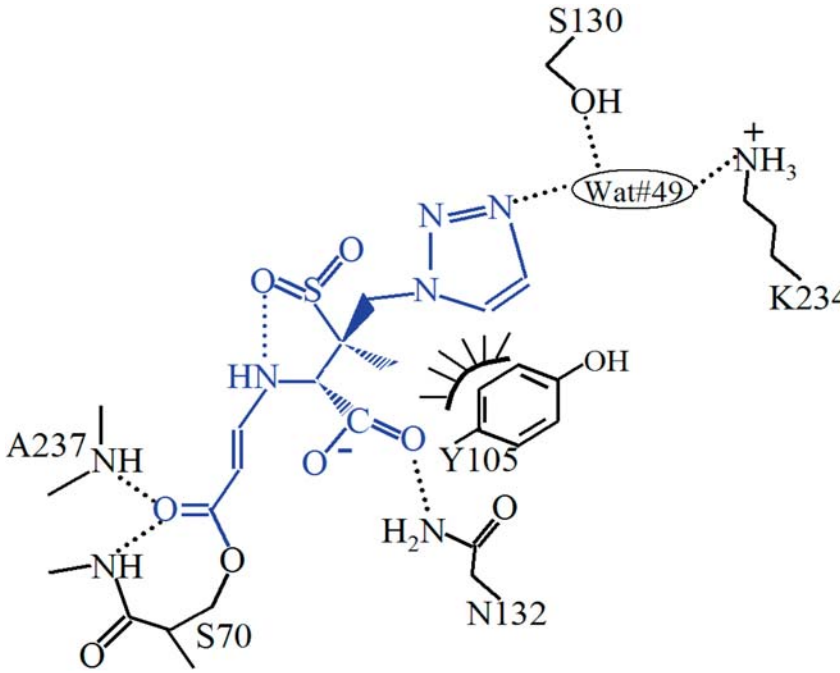

Scheme 4 A diagram of tazobactam bound to the E166A mutant of SHV-1 β-lactamase. Hydrogen bonds are highlighted as dotted lines, and the hydrophobic van der Waals interactions between Y105 and the triazolyl ring and methyl moieties of tazobactam are depicted by the hatched curved line.

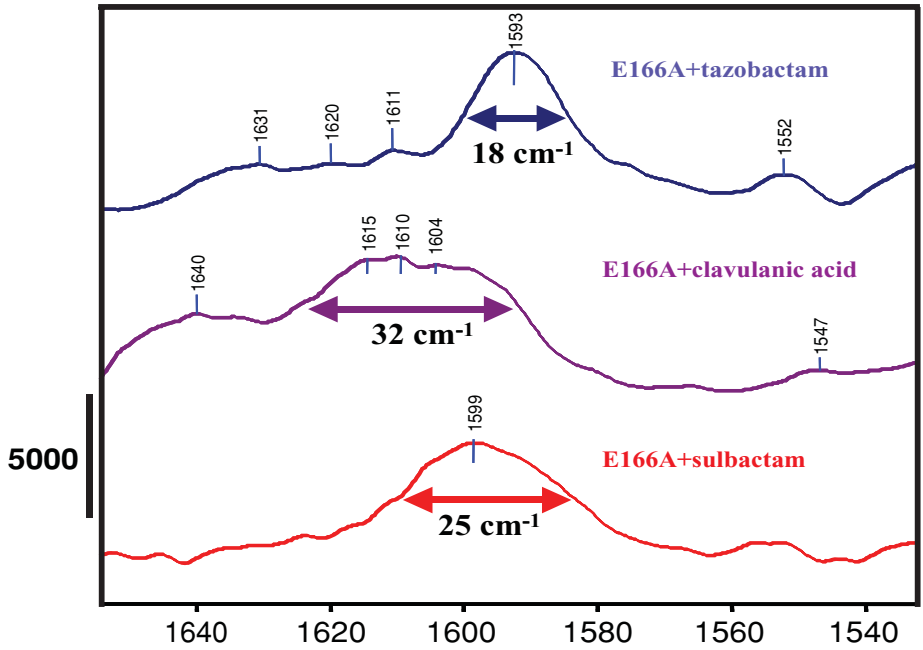

Figure 5 Partial Raman difference spectra for the *trans*-enamine intermediates showing the band profile for the –NH-C═C-C(═O) stretching frequency.

This may explain in part why tazobactam is a superior inhibitor; it may form a more stable enamine and thus more effectively block the active site. The synergy between spectroscopy and crystallography is further exemplified by a comparison of the enamine intermediates formed by the three suicide inhibitors shown in Scheme 2. For the three inhibitors, Figure 5 compares the band profiles of the main enamine symmetric stretching frequency near 1595 cm^{-1}, from the Raman difference data. The bandwidths at half height are 18, 25, and 32 cm^{-1} for the intermediates formed from tazobactam, sulbactam, and clavulanic acid, respectively. Increasing bandwidth is interpreted in terms of increasing conformational heterogeneity (30); i.e., although both sulbactam and clavulanic acid form *trans*-enamines in the active site, there is conformational variability about this mean structure, either in the static or dynamic sense. This finding is perfectly mirrored by the X-ray crystallographic results; although the enamine from tazobactam forms the single well-defined population (Scheme 4), those from sulbactam and clavulanic acid are quite different in that the electron density becomes essentially invisible for the main inhibitor chain beyond the –NH- moiety (Scheme 3). That is, there is extensive static or dynamic disorder in the two tail regions that include the –NH- and beyond. This is the cause of the line broadening seen in Figure 5. The interplay between the Raman and X-ray data is exemplified in Figure 6; there

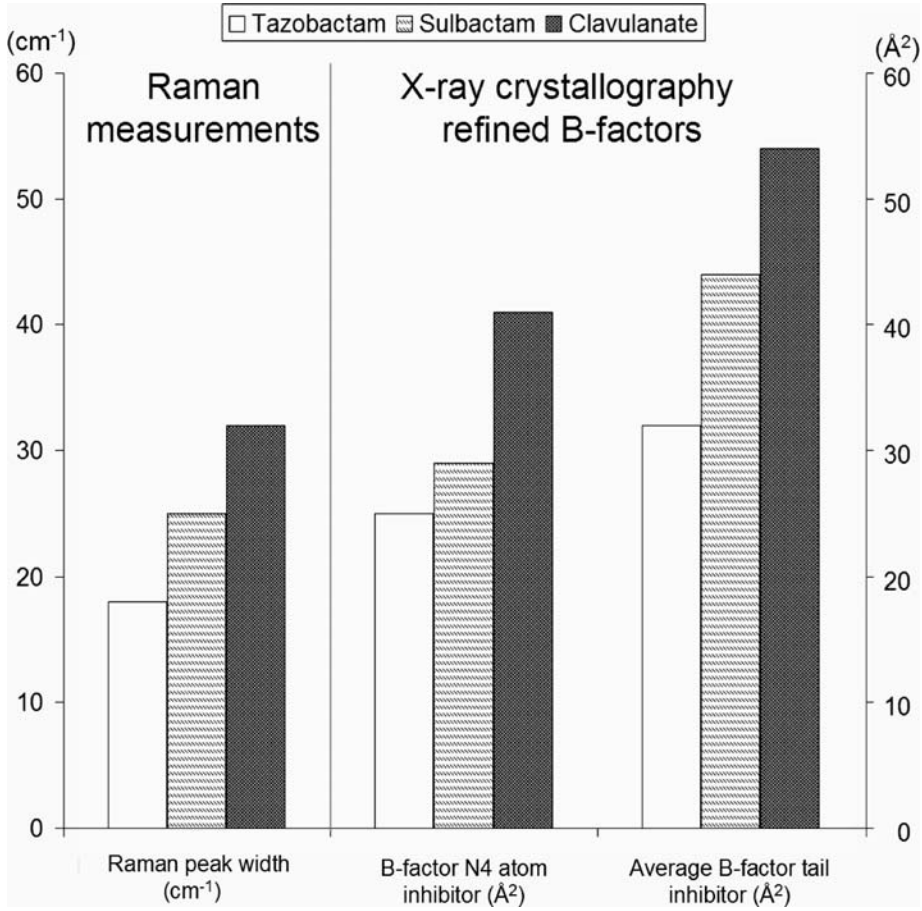

Figure 6 Raman bandwidths for the features seen in Figure 5 and B-factors from the X-ray analysis. The B-factors are plotted for the N4 atom alone and for the tail atoms (those beyond N4).

the trend in Raman linewidths of the enamine features is exactly mirrored by the increase in crystallographic B-factors for the N4 atom and for all the tail atoms (i.e., those beyond N4) (31). The increase in the B-factors denotes increase in the mobility of the atoms.

Unique Applications of Raman Crystallography

Thus far, two areas of Raman crystallography have offered unique opportunities. In one, echoing Yu's earlier studies (9), Raman crystallography has been used to compare the properties of proteins in crystals and in solution. The second application has no precedent and concerns the discovery that proteins in single

crystals can undergo enormous irreversible changes in their secondary structure with the majority of peptide bonds becoming involved in β-sheet structure.

COMPARING PROTEIN PROPERTIES IN SINGLE CRYSTALS AND IN SOLUTION Since the dawn of macromolecular crystallography half a century ago, there have been arguments about how closely structures derived from single crystals resemble those found in more biologically relevant conditions—in solution. In his pioneering studies, Yu showed that there is no evidence for changes in secondary structure when α-lactoglobulin, for example, goes from the crystalline state to aqueous solution (9). Using Raman crystallography, we can now also ask if protein-ligand interactions vary between crystalline and solution complexes. The enzyme *para*-hydroxybenzoate hydroxylase (PHBH) makes an intriguing case study because its flavin cofactor migrates between two sites on the protein during the catalytic cycle (32). In one site, the "in" conformation (Figure 7), the flavin's isoalloxazine ring is buried in a protein pocket. This form is present when the substrate 4-hydroxybenzoic acid (*p*-OHB) binds to PHBH. In contrast, when the substrate analog 2,4-dihydroxybenzoic acid (2,4-diOHB) binds, the flavin ring is forced into the "out" conformation (Figure 7) where it is surrounded by water molecules. The Raman spectra for the isoalloxazine ring modes are compared for the in and out forms in Figure 7, where marked differences can be seen (19, 33). Examination of the Raman marker bands for the in conformers in the solution and crystalline forms of the enzyme revealed that they are indistinguishable. However, there are small but significant differences in the positions of the out marker bands (19). These differences were ascribed to differences in the structure of the water molecules surrounding the flavin ring in solution and in the crystal. In a theme that echoes the discussion on enamine-β-lactamase line widths above, another general difference between the flavin modes from PHBH in solution and single crystals is that crystallization results in a narrowing of the band profiles—by up to 30%. The narrowing is interpreted in terms of the protein being more restrained in its dynamical movements in the crystalline phase, and thus the flavin ring exists in a more limited range of closely related conformational states in the crystal than in solution.

The relationship between Raman line widths and protein dynamics has been explored further for insulin molecules (34). Insulin, with a 5.8-kDa MW, normally exists as a hexamer, but mutant forms can result in the appearance of entirely dimeric or monomeric species in solution. The amide I profile was taken as a measure of conformational heterogeneity, with line broadening attributed to a wider range of rapidly interconverting conformational states. The amide I profile narrows progressively going from monomer (bandwidth at half height $= 54\,\mathrm{cm}^{-1}$), to dimer ($48\ \mathrm{cm}^{-1}$), to hexamer in solution ($42\ \mathrm{cm}^{-1}$), and finally to hexamer in the crystalline phase ($37\ \mathrm{cm}^{-1}$). This effect was ascribed to the progressive mechanical damping of insulin chain fluctuations with increasing insulin assembly (34).

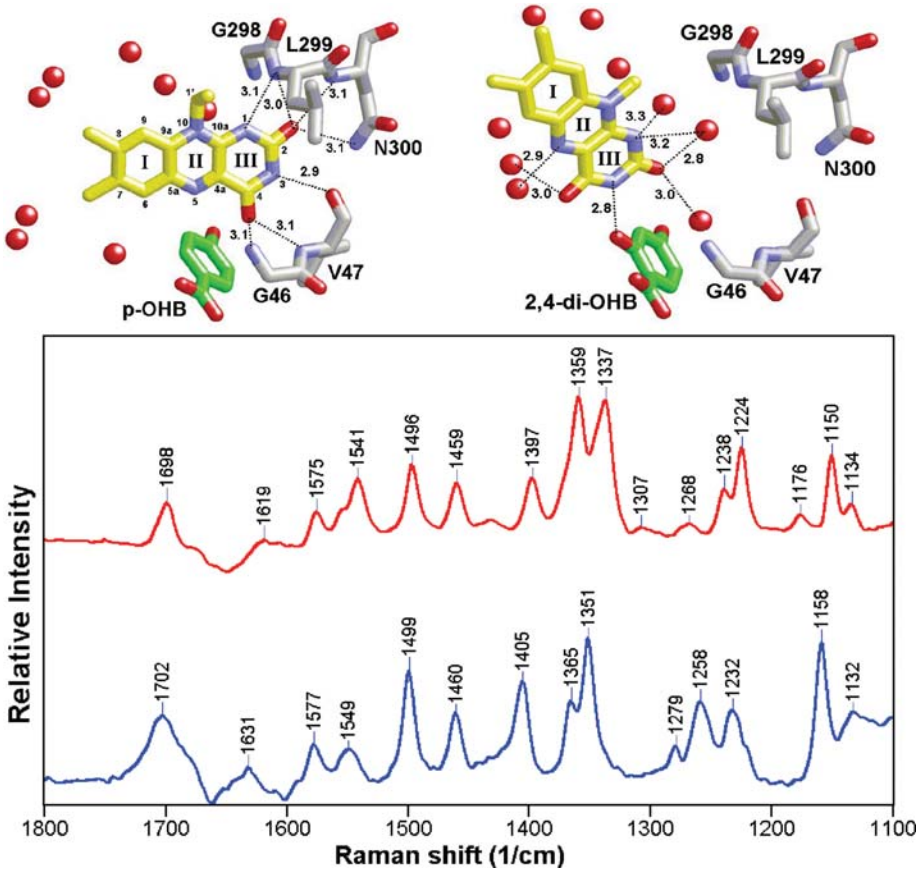

Figure 7 (*Top*) Structures of the active sites of the PHBH complexes. Putative hydrogen bonds are depicted with dotted lines, and water molecules are shown as red spheres. (*Left*) Holo-PHBH plus *p*-OHB (in conformation); (*Right*) holo-PHBH plus 2,4-di-OHB (out conformation). Structures were obtained from the Protein Data Bank [PDB code 1PBE and 1DOD for holo-PHBH plus *p*-OHB (in) and holo-PHBH plus 2,4-di-OHB (out), respectively]. (*Bottom*) Raman difference spectra for FAD bound to wild-type PHBH single crystal. (*Top*) Holo-PHBH plus *p*-OHB (in); (*Bottom*) holo-PHBH + 2,4-di-OHB (out).

MASSIVE CONFORMATIONAL CHANGES WITHIN CRYSTALS The precise positions of Raman amide I and III bands are characteristic for β-sheet and α-helical secondary structures, and, in addition, α-helices show characteristic Raman intensities near 1340 and 940 cm^{-1}. Thus, it is trivial to identify these marker bands in single-crystal spectra. In 2000 our laboratory began Raman crystallographic studies on transcarboxylase's second major subunit, the so-called 5S, a 120 kDa dimer that converts bound pyruvate to oxaloacetate using $–CO_2^-$ from carboxybiotin (21).

We were puzzled by the observation that the secondary structure Raman markers appeared to be different for 5S from crystal to crystal. This varied so greatly from our experience with many other crystal samples that we ignored the problem for some time. However, the underlying cause of the apparent variation in secondary structure was subsequently identified. The crystals grown at pH 7.0 showed a clear mixture of β-sheet and α-helical secondary structure Raman markers, and this was confirmed by subsequent X-ray crystallographic analysis (35). But once the pH in the surrounding mother liquor was dropped to 4.5, the intensity of the α-helical markers declined dramatically, whereas those due to β-sheet increased (36). Figure 8 shows the decrease in the characteristic α-helical feature near 940 cm^{-1} over a period of 4 h after the pH around the crystal had been reduced to 4.5. This conversion appears to be irreversible.

Subsequently, we showed similar effects for other proteins, but using different sets of perturbants. Insulin is approximately 50% α-helical, but when the -S-S- linkages in the crystal are reduced to –SH by infusing in a chemical-reducing

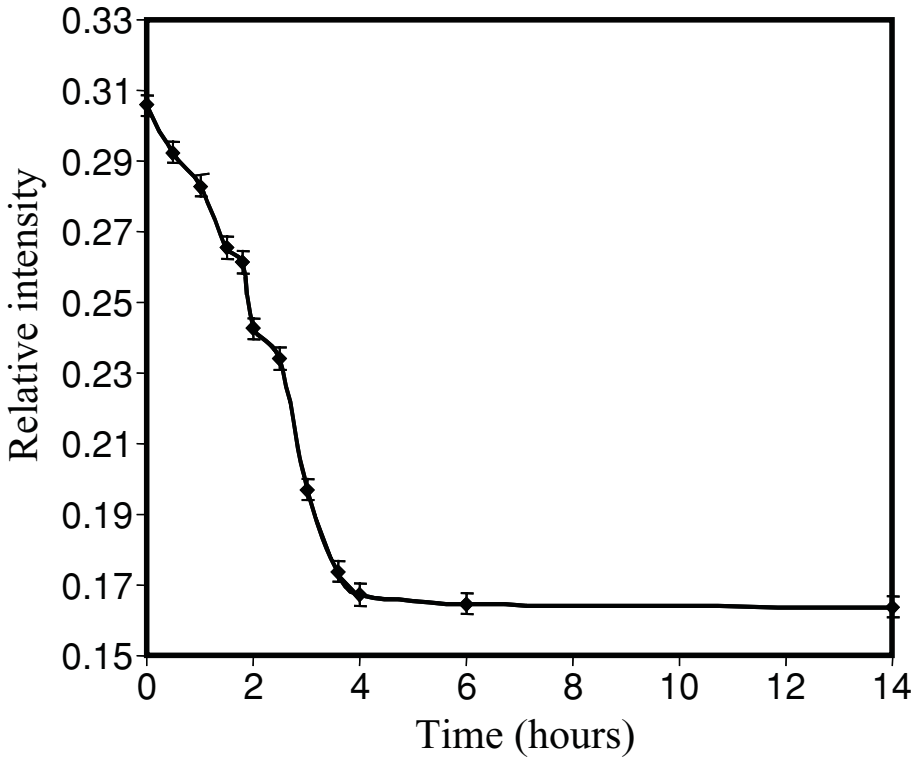

Figure 8 Time-dependent changes of Raman intensity at the helix marker band at 940 cm^{-1} from the 5S subunit of transcarboxylase after reducing the pH from 6.5 to 4.5. The Raman intensity at 1450 cm^{-1} is used as reference.

agent, all α-helical markers disappear from the Raman spectrum of the crystal to be replaced by β-sheet bands. The behavior of the 12S subunit, from the multisubunit enzyme transcarboxylase, is even more bizarre (36). 12S crystals do not appear to be sensitive to pH changes, and they undergo only small reversible conformational changes upon binding the substrate MM-CoA. However, when both substrates, MM-CoA and biotin, are added to the mother liquor around 12S crystals, the protein converts from a mixture of α-helix and β-sheet to entirely β-sheet.

Though we are far from a full understanding of the mechanics of these wholesale conformational changes, all three proteins examined thus far, 5S, insulin, and 12S, share the same properties in their β-sheet converted forms:

- The change to predominantly β-sheet is irreversible.
- The crystal morphology appears unchanged, but it no longer diffracts X rays.
- The crystal's solubility is greatly diminished.
- The converted crystals can be stained with Congo red and thioflavin S, whereas the native crystals cannot.

These factors suggest that proteins in crystals can undergo relatively massive conformational changes to form β-sheet secondary structure and that intermolecular sheets are likely formed. The effect occurs rarely, is catalyzed by widely divergent conditions, and is difficult to characterize by any other means apart from Raman microscopy, mostly owing to the loss of solubility and diffraction. The observed changes are not a result of a rise in temperature caused by laser beam; the temperature in the hanging drop increases by approximately 10°C during irradiation, but the conformational changes occur only after adding the appropriate chemical perturbant.

PROTEIN MISFOLDING RELATED TO ALZHEIMER'S AND PARKINSON'S DISEASES

The polypeptide chains of most proteins have the ability to fold into a unique three-dimensional structure that confers biological function. Moreover, many proteins, however irregular in shape, can be coaxed into forming perfectly periodic three-dimensional arrays. Such single crystals are the topic of the first part of this review. However, it is becoming increasingly apparent that many proteins also have the property of misfolding to form fiber-like strands where β-sheet secondary structure predominates. We demonstrate above that β-sheet conversion can occur in single crystals that begin as perfect native structures. Now we consider protein misfolding in a more medical context. Because protein misfolding underlies the pathology of several disease states, it is a topic of intense interest. This is particularly true for neurodegenerative conditions such as Alzheimer's and Parkinson's diseases. Recent reports demonstrate that Raman microscopy can contribute to this field in at least two ways. It can characterize the chemistry of protein-based

deposits found in the brains of patients who have died from a neurogenerative disease. Moreover, in a more fundamental sense, in vitro it can characterize intermediates on the protein misfolding pathway and thus contribute to our knowledge of how the protein deposits are formed in the brain.

Isolated Senile Plaque Cores Associated with Alzheimer's Disease

Neurodegenerative diseases are defined pathologically by the aggregation of protein in deposits such as senile plaques (SPs), neurofibrillary tangles, and Lewy bodies. Compositional analyses have shown that SP cores in Alzheimer's disease consist of a 42 peptide protein known as Aβ and numerous other associated protein and nonprotein components (37). The relative contribution of these components to amyloid deposits and the structural characteristics of SP cores, however, remain unknown. Using a Raman microscope, researchers can obtain high-quality Raman data from SP cores that had been isolated from the brains of deceased Alzheimer's patients. The cores were typically 10 microns in size and were examined dried on aluminum or silver foil.

The Raman spectrum of a single SP core is shown in Figure 9. Detailed analysis is made possible by reference to the literature on the Raman spectra of proteins,

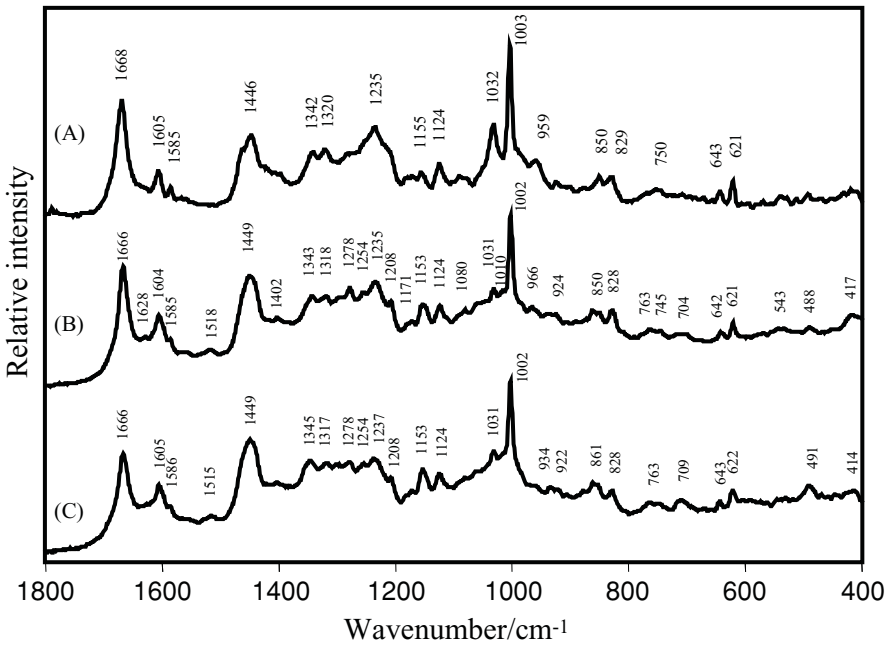

Figure 9 Raman spectra of (*A*) synthetic Aβ(1–42) fibrils, (*B*) senile plaque core, and (*C*) senile plaque core treated with 2.5 mM EDTA (pH 7.0) for 24 h.

by the availability of synthetic fibrils made from Aβ(1–42) peptide (Figure 9), and by a number of Raman studies undertaken by Miura, Takeuchi, and colleagues on the interactions of synthetic Aβ with metals (38). The main conclusions can be summarized (39) as follows:

- The close resemblance between Figures 9*A* and *B* indicates that Aβ is the main component of the SP.
- The amide I and III conformation marker bands at 1666 and 1235 cm^{-1}, respectively, show that the Aβ protein is predominantly in a β-sheet secondary structure, possibly as a parallel β-helix.
- The Raman data are similar for SPs from the same brain and for SPs from three different brains.
- Raman bands characteristic of methionine sulfoxide show that extensive methionine oxidation has occurred at some stage of formation of the intact plaques.
- Marker bands due to imidazole modes demonstrate that histidine side chains in the Aβ protein are coordinated to Zn(II) and Cu(II). Treatment of the SPs with the chelator ethylenediamine tetraacetate reverses Cu binding to SP histidines and leads to a broadening of amide features indicating a loosening of the β-structure (Figure 9). This result has attracted attention because it implies that the process of β-sheet formation may, in part, be reversible.

It must be emphasized that most of this information is completely new and demonstrates the power of Raman microscopy to elicit detailed chemical information on a complex biological particle. It works well in the present example because, fortuitously, the SP is essentially homogeneous; although it has a number of minor components, it is composed predominantly of a single protein.

Characterizing α-Synuclein and Intermediates

α-Synuclein is an abundant, small (140 amino acids) presynaptic protein that belongs to a larger family of proteins including β- and γ-synuclein. The synucleins are prototypical members of the class of natively unfolded proteins. In the latter the protein is not folded into a compact, defined conformation but is more chain-like as evidenced by high hydrodynamic radii. Typically natively unfolded proteins possess only a small amount of secondary structure. However, α-synuclein can aggregate to form fibrils. This process is of high interest because α-synuclein fibrils are the major component of Lewy bodies, the intracytoplasmic inclusions that are the neuropathological hallmark of Parkinson's disease (40). Raman microscopy, combined with atomic force microscopy, has been able to provide insight into the aggregation and fibrilization of α-synuclein.

In an initial study, Maiti et al. (41) showed that the amide I band profiles of several natively unfolded proteins including α-synuclein could be fitted by three bands:

- A band near 1650 cm^{-1} that emanates from residues in Ramachandran α-helical space. Few or no lengths of extended α-helix may be present, but, e.g., transient di- or tri-peptide sequences whose φ,Ψ angles are in helical space will contribute to the 1650 cm^{-1} feature.
- A band near 1665 cm^{-1} that derives from β-sheet structure. For natively unfolded proteins, this is a minor contribution to the overall profile.
- A band near 1680 cm^{-1} that is due to peptide residues that are in Ramachandran β-space but that are not forming interstrand hydrogen bonds. Thus, β-strands and polyproline II structures meet this criterion.

This simple band-fitting procedure could be used to characterize the secondary structure of α-synuclein in solution and to follow changes in the structure in the presence of methanol (a β-sheet forming agent) or hexafluoro-2-propanol (an α-helix forming agent).

In subsequent work, Apetri et al. (42) used the same amide I band fitting procedure, combined with atomic force microscopy analysis, to follow the process of fibrilization. Aqueous samples of α-synuclein were incubated at 37°C for long periods of time—involving several weeks. The resulting oligomers were deposited on a mica surface and examined by atomic force microscopy. As can be seen in Figure 10, spherical oligomers were observed after 21 days, spherical oligomers and protofilaments after 32 days, and filaments after 42 days of incubation. The same samples, on the mica platform, were also examined under the Raman microscope, and analysis of the amide I profile gave the secondary structure composition of the species identified by atomic force microscopy. The oligomers have a substantial population of peptide residues in α-helical space, but this decreases, along with the polyproline II-like population, as the protofilaments mature and is replaced by residues in β-sheet structures. This is the first time that a direct link has been established between particle morphology and secondary structure.

FUTURE TRENDS

An important advance for Raman crystallography would be the introduction of a high-light throughput (i.e., more sensitive) Raman microscope that significantly reduces the time for data collection. At this time it takes approximately 100 seconds to record an acceptable Raman spectrum from a crystal working in a nonconfocal mode using 100 mW of 647 nm laser excitation. If data could be collected in a shorter time in a confocal mode, the small effective focal volume would also reduce problems associated with the so-called onion effect—namely, that molecules diffusing into crystals arrive at the outside layers before they reach the center. This is a concern as more rapid reactions are studied within the crystal environment. As data collection times become smaller, effort will need to be expended to start reactions synchronously throughout the crystal. Using a second laser system to start a reaction in the crystal photochemically, with a photo-activated substrate already in position in or near the active site, is a possibility.

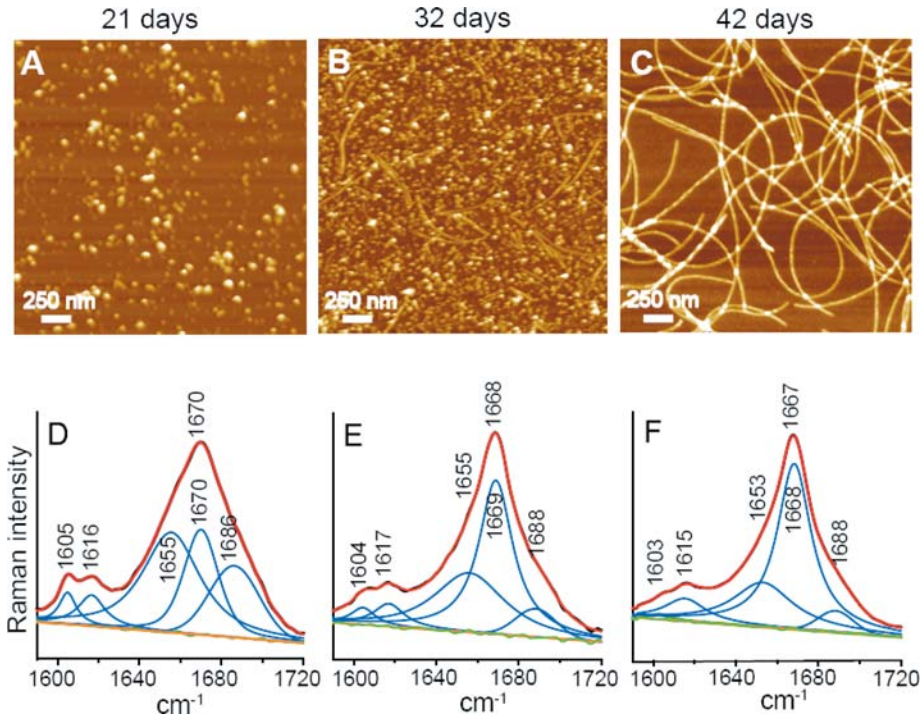

Figure 10 (*Top*) Atomic force microscopic images of α-synuclein on a mica surface: (*A*) spherical oligomers, (*B*) spherical oligomers and protofilaments, and (*C*) filaments. (*Bottom*) The amide I profile (Raman spectrum) with band fitting of the same samples: (*D*) spherical oligomers, (*E*) spherical oligomers and protofilaments, and (*F*) filaments.

High-quality Raman spectra can be collected from single protein crystals kept at very low temperatures (near 100 K) in a stream of cold nitrogen gas using the method employed by X-ray crystallographers to keep flash-frozen crystals cold in the X-ray beam (P. Carey & N. Maiti, unpublished data). Thus, it will be possible to compare conformational populations at room temperature and at very low temperature and characterize the consequences of flash freezing.

The coexistence of spectroscopic data and high-resolution X-ray crystallographic data for enzyme-substrate complexes provides an excellent opportunity to undertake high-level quantum-mechanical and molecular mechanics calculations on these complexes, that, in a sense, act as a test bed for these calculations.

Other areas of macromolecular crystallography such as DNA-protein complexes, RNA-based ribozymes, and membrane proteins are in an active state of development. For these, Raman crystallography has the potential of acting as a pathfinder and providing synergistic data in the same manner as for more simple proteins.

ACKNOWLEDGEMENTS

The author is grateful to his colleagues and collaborators who have contibuted to the research described above. Their names appear in the list of references. The work is supported by the National Institutes of Health (GM 54072 and DK 53053).

LITERATURE CITED

1. Puppels GJ. 1999. Confocal Raman microspectroscopy. In *Fluorescent and Luminescent Probes for Biological Activity*, ed. WT Mason, p. 377. New York: Academic. 2nd ed.
2. Cheng J-X, Xie XS. 2004. Coherent anti-Stokes Raman scattering microscopy: instrumentation, theory, and applications. *J. Phys. Chem. B* 108:827–40
3. Pearson AR, Mozzarelli A, Rossi GL. 2004. Microspectrophotometry for structural enzymology. *Curr. Opin. Struct. Biol.* 14:656–62
4. Sage JT. 1997. Infrared crystallography: structural refinement through spectroscopy. *J. Appl. Spectrosc*. 51:568–73
5. Carey PR, Dong J. 2004. Following ligand binding and ligand reactions in proteins via Raman crystallography. *Biochemistry* 43:8885–93
6. Carey PR, Tonge PJ. 1995. Unlocking the secrets of enzyme power using Raman spectroscopy. *Acc. Chem. Res.* 28:8–13
7. Carey PR. 1999. Raman spectroscopy, the sleeping giant in structural biology, awakes. *J. Biol. Chem.* 274:26625–28
8. Deng H, Callender RH. 1999. Raman spectroscopic studies of the structures, energetics, and bond distortions of substrates bound to enzymes. *Methods Enzymol*. 308:176–201
9. Yu N-T. 1974. Comparison of protein structure in crystals, in lyophilized state, and in solution by laser Raman scattering. 3. α-lactalbumin. *J. Am. Chem. Soc.* 96:4664–68, and references cited therein.
10. Zhu L, Sage JT, Champion PM. 1993. Quantitative structural comparisons of heme protein crystals and solutions using resonance Raman spectroscopy. *Biochemistry* 32:11181–85
11. Morikis D, Sage JT, Rizos AK, Champion PM. 1988. Resonance Raman studies of myoglobin single-crystals. *J. Am. Chem. Soc.* 110:6341–42
12. Loppnow G, Barry B, Mathies R. 1989. Why are blue visual pigments blue? A resonance Raman microprobe study. *Proc. Natl. Acad. Sci. USA* 86:1515–18
13. Puppels GJ, de Mul FF, Otto C, Greve J, Robert-Nicoud M, et al. 1990. Studying single living cells and chromosomes by confocal Raman microspectroscopy. *Nature* 347:301–3
14. Smulevich G, Spiro TG. 1993. Single-crystal micro-Raman spectroscopy. *Methods Enzymol.* 226:397–408
15. Li T, Chen Z, Johnson JE, Thomas GJ. 1992. Conformations, interactions, and thermostabilities of RNA and proteins in bean pod mottle virus: investigation of solution and crystal structures by laser Raman spectroscopy. *Biochemistry* 31:6673–82
16. Benevides JM, Terwilliger TC, Vohnik S, Thomas GJ. 1996. Raman spectroscopy of the Ff gene V protein and complexes with poly(dA): nonspecific DNA recognition and binding. *Biochemistry* 35:9603–9
17. Thomas GA, Kubasek WL, Peticolas WL, Greene P, Grable J, Rosenberg JM. 1989. Environmentally induced conformational changes in B-type DNA: comparison of

the conformation of the oligonucleotide d(TCGCGAATTCGCG) in solution and in its crystalline complex with the restriction nuclease EcoRI. *Biochemistry* 28:2001–9

18. Tonge PJ, Carey PR, Callender R, Deng H, Ekiel I, Mulhandiram DR. 1993. Characterization of *trans* and *cis* 5-methylthienylacryloyl-chymotrypsin using Raman difference spectroscopy, NMR and kinetics: carbonyl environment and reactivity. *J. Am. Chem. Soc.* 115:8757–62
19. Altose MD, Zheng Y, Dong J, Palfey BA, Carey PR. 2001. Comparing protein-ligand interactions in solution and single crystals by Raman spectroscopy. *Proc. Natl. Acad. Sci. USA* 98:3006–11
20. Tsuboi M, Thomas GJ. 1997. Raman scattering tensors in biological molecules and their assemblies. *Appl. Spectrosc. Rev.* 32:263–99
21. Wood HG, Zwolinski G. 1976. Transcarboxylase: role of biotin, metals, and subunits in the reaction and its quaternary structure. *CRC Crit. Rev. Biochem.* 4:47–122
22. Hall PR, Wang YF, Rivera-Hainaj RE, Zheng XJ, Pusztai-Carey M, et al. 2003. Transcarboxylase 12S crystal structure: hexamer assembly and substrate binding to a multienzyme core. *EMBO J.* 22:2334–47
23. Zheng X, Rivera-Hainaj RE, Zheng Y, Pusztai-Carey M, Hall PR, et al. 2002. Substrate binding induces a cooperative conformational change in the 12S subunit of transcarboxylase: Raman crystallographic evidence. *Biochemistry* 41:10741–46
24. Helfand MS, Totir MA, Carey MP, Hujer AM, Bonomo RA, Carey PR. 2003. Following the reactions of mechanism-based inhibitors with β-lactamase by Raman crystallography. *Biochemistry* 42:13386–92
25. Dong J, Wan Z-L, Chu Y-C, Nakagawa SN, Katsoyannis PG, et al. 2001. Isotope-edited Raman spectroscopy of proteins: a general strategy to probe individual peptide bonds with application to insulin. *J. Am. Chem. Soc.* 123:7919–20
26. Dong J, Swift K, Matayoshi E, Nienaber VL, Weitzberg M, et al. 2001. Probing inhibitors binding to human urokinase crystals by Raman microscopy: implications for compound screening. *Biochemistry* 40:9751–57
27. Helfand MS, Bonomo RA. 2003. β-Lactamases: a survey of protein diversity. *Curr. Drug Targets Infect. Disord.* 3:9–23
28. Page MG. 2000. β-Lactamase inhibitors. *Drug Resist. Updates* 3:109–25
29. Padayatti PS, Helfand MS, Totir MA, Carey MP, Hujer AM, et al. 2004. Tazobactam forms a stoichiometric *trans*-enamine intermediate in the E166A variant of SHV-1 β-lactamase: 1.63 Å crystal structure. *Biochemistry* 43:843–48
30. Carey PR, Froese A, Schneider H. 1973. Resonance Raman spectroscopic studies of 2,4-dinitrophenyl hapten-antibody interactions. *Biochemistry* 12:2198–208
31. Padayatti PS, Helfand MS, Totir MA, Carey MP, Carey PR, et al. 2005. High resolution crystal structures of the *trans*-enamine intermediates formed by sulbactam and clavulanic acid and E166A SHV-1 β-lactamase. *J. Biol. Chem.* 280:34900–7
32. Palfey B, Massey V. 1998. Flavin-dependent enzymes. In *Comprehensive Biological Catalysis, A Mechanistic Reference.* Vol. 3: *Radical Reactions and Oxidation/Reduction*, ed. M Sinnott, pp. 83–154. San Diego: Academic
33. Zheng YG, Dong J, Palfey BA, Carey PR. 1999. Using Raman spectroscopy to monitor the solvent-exposed and "buried" forms of flavin in *p*-hydroxybenzoate hydroxylase. *Biochemistry* 38:16727–32
34. Dong J, Wan ZL, Popov M, Carey PR, Weiss MA. 2003. Insulin assembly damps conformational fluctuations: Raman analysis of amide I linewidths in native states and fibrils. *J. Mol. Biol.* 330:431–42
35. Hall PR, Zheng R, Antony L, Pusztai-Carey M, Carey PR, Yee V. 2004. Transcarboxylase 5S structures: assembly and catalytic mechanism of a multienzyme complex subunit. *EMBO J.* 23:3621–31

36. Zheng R, Zheng X, Dong J, Carey PR. 2004. Proteins can convert to β-sheet in single crystals. *Protein Sci.* 13:1288–94
37. Atwood CS, Martins RN, Smith MA, Perry G. 2002. Senile plaque composition and posttranslational modification of amyloid-beta peptide and associated proteins. *Peptides* 23:1343–50
38. Miura T, Suzuki K, Kohata N, Takeuchi H. 2000. Metal binding modes of Alzheimer's amyloid β-peptide in insoluble aggregates and soluble complexes. *Biochemistry* 39:7024–31
39. Dong J, Atwood CS, Anderson VE, Siedlak SL, Smith MA, et al. 2003. Metal binding and oxidation of amyloid-β within isolated senile plaque cores: Raman microscopic evidence. *Biochemistry* 42:2768–73
40. Spillantini MG, Schmidt ML, Lee VM, Trojanowski JQ, Jakes R, Goedert M. 1997. Alpha-synuclein in Lewy bodies. *Nature* 388:839–40
41. Maiti NC, Apetri MM, Zagorski MG, Carey PR, Anderson VE. 2004. Raman spectroscopic characterization of secondary structure in natively unfolded proteins: α-synuclein. *J. Am. Chem. Soc.* 126:2399–2408
42. Apetri MM, Maiti NC, Zagorski MG, Carey PR, Anderson VE. 2006. Secondary structure of α-synuclein monomers: characterization by Raman and atomic force microscopy. *J. Mol. Biol.* 355:63–71